8-26-2015

Carbon Dioxide Sorption in a Nanoporous Octahedral Molecular Sieve

Izaak Williamson
Boise State University

Eric B. Nelson
Boise State University

Lan Li
Boise State University

Carbon Dioxide Sorption in a Nanoporous Octahedral Molecular Sieve

Izaak Williamson
Department of Materials Science and Engineering
Boise State University
Boise, ID

Eric B. Nelson
Department of Materials Science and Engineering
Boise State University
Boise, ID

Lan Li
Department of Materials Science and Engineering
Boise State University
Boise, ID

ABSTRACT

We have performed first-principles density functional theory calculations, incorporated with van der Waals interactions, to study CO_2 adsorption and diffusion in nanoporous solid – OMS-2 (Octahedral Molecular Sieve). We found the charge, type, and mobility of a cation, accommodated in a porous OMS-2 material for structural stability, can affect not only the OMS-2 structural features but also CO_2 sorption performance. This paper targets K^+, Na^+, and Ba^{2+} cations. First-principles energetics and electronic structure calculations indicate that Ba^{2+} has the strongest interaction with the OMS-2 porous surface due to valence electrons donation to the OMS-2 and molecular orbital hybridization. However, the Ba-doped OMS-2 has the worst CO_2 uptake capacity. We also found evidence of sorption hysteresis in the K- and Na-doped OMS-2 materials.

I. Introduction

The capture and storage of carbon dioxide from fossil fuel power plant emissions are important tasks that scientists are facing today [1]. Research has shown that adsorption of CO_2 onto solids can be an effective method for selectively separating CO_2 from flue gases [2-7]. This method has a lower parasitic energy than current aqueous technologies and could potentially replace them [6,8-11]. Porous solids, including zeolite membranes, molecular sieves, and metal organic frameworks are preferential for gas adsorption because of their high surface areas [4-7,12-18]. These materials can have a variety of pore geometries and sizes which can affect the CO_2 adsorption and desorption properties [6,19-22]. There is also the potential for further "tuning" of the properties by chemical substitution making these great candidates for 'materials-by-design' applications [5,6,9,18]. Extensive computational studies confirm the need to explore the structural behavior of CO_2 with an analysis of relative van der Waals (vdW) bonding for metal organic framework candidates [2,6,17,18,23,24]. However, many of these materials experience hysteresis in their adsorption and desorption processes which increase the parasitic energy. Understanding the mechanism behind this hysteresis is necessary for advancing these materials into industrial applications.

Manganese dioxide α-MnO_2, referred to as OMS-2, is a nanoporous octahedral molecular sieve (OMS) that experiences CO_2 hysteresis [21,22,25]. The framework of the OMS-2 structure is made up of edge-sharing MnO_6 octahedra that form relatively small (1×1) and large (2×2) tunnels. These tunnels act as one-dimensional "traps" where CO_2 adsorption and molecular sieving processes can occur[2]. The OMS-2 structure requires the presence of cations inside the large (2×2) tunnels that act as a means of structural support. Common dopants for this system

include K^+, Ba^{2+}, Na^+, and Pb^{4+} [21,22,25]. Previously, we found that adding K^+ ions to the (2×2) tunnels leads to hysteresis looping in the adsorption and desorption isotherms [26]. The onset of hysteresis only occurs at experimental partial pressures exceeding 7 bar (700 kPa). This study revealed the importance of understanding the CO_2 sorption mechanism and the physical factors involved.

Density functional theory (DFT) calculations with van der Waals forces revealed CO_2 sorption on K-doped OMS-2, known as cryptomelane [27]. We investigated the diffusion of CO_2 through the (2×2) tunnel and found that the K^+ dopant acts as a 'gate keeper' blocking the path of the CO_2 molecules. When the concentration of CO_2 is increased (>7 bar pressure), the activation energy barrier for the CO_2 to bypass K^+ reduces significantly. This allows the CO_2 to become trapped behind K^+, hindering desorption. More recently, we compared the sorption behavior of Ba-doped OMS-2, known as hollandite, to the results from cryptomelane [9]. The higher-charge cation Ba^{2+} was found to perform worse in the CO_2 sorption than the lower-charge cation K^+. This could be attributed to the stronger binding energy of Ba^{2+} with the OMS-2 porous surface.

In further studying the cation effect, this paper compares K^+, Na^+, and Ba^{2+} cations in the OMS-2, including their structural features, interactions with the pore surface, and CO_2 adsorption and diffusion mechanisms. These studies identify key factors controlling CO_2 uptake capacity and help develop high-performance porous solids for carbon capture and storage.

II. Computational Methods

The Vienna *ab-initio* Software Package (VASP)[28] was performed within density functional theory (DFT) to conduct all structural, energetic, and electronic structure calculations. The spin-polarized generalized gradient approximation (GGA) was used within the Perdew Burke Ernzerhoff formalism revised for solid systems (PBEsol)[29]. The plane-wave basis sets were expanded using projector-augmented wave (PAW) pseudopotentials[30,31] to a cutoff energy of 400eV. To account for the d-orbitals of Mn, the GGA+U approach of Liechtenstein *et al* [32] was employed, where an effective on-site Coulomb potential (U) of 2.8eV and an exchange potential (J) of 1.2eV were applied to the system. The Brillouin zone integration was performed on a 6x6x6 Monkhorst-Pack mesh. To account for Fermi surface broadening, a Gaussian smearing value of 0.05eV was applied. The Mn atoms have an antiferromagnetic interaction with magnetic moments of $\pm 4\ \mu_B$.[33,34] All relaxations of the lattice parameters and atomic positions were performed until residual forces were reduced to 0.01eV/Å. In a previous study[34], we found that incorporating van der Waals (vdW) forces using the DFT-D2 approach of Grimme,[35] applied to the α-MnO_2 structure accommodating K^+ and H_2O, produced a binding energy very similar to that of the DFT calculation. The charge and dipole interactions were found to dominate in this system. Although, it has been shown that the electrostatic interactions dominate when CO_2 is near a cation [36] and vdW interactions are prominent when CO_2 is far from the cation (away from its equilibrium position) [37]. Nevertheless, we incorporated the vdW-DFT scheme in the energetic calculations to compare with DFT. In addition, we performed nudged elastic band method to confirm a transition state during CO_2 diffusion in the OMS-2.

The unit cell of α-MnO_2 (with no cation) is Mn_8O_{16} with calculated equilibrium lattice parameters, a = 9.702Å, b = 2.856Å, and c = 9.685Å. In order to accommodate the cations and CO_2 molecules in the (2×2) tunnel, we tripled the unit cell along the b axis. The 1x3x1 supercell was found to be energetically favorable and was used to elongate the tunnels formed by the edge-sharing MnO_6 octahedra. We used the cell of $XMn_{24}O_{48}$ (i.e. $X_{0.04}MnO_2$), where X = K, Na, or Ba, and varied CO_2 concentration in the cell to provide insight into the CO_2 sorption mechanism.

III. Results and Discussion

K^+, Na^+, and Ba^{2+} Cations

The equilibrium parameters of undoped 1x3x1 α-MnO_2 supercell (i.e. with no cation) are a = 9.702 Å, b = 8.568 Å, c = 9.685 Å. The dopants were then added manually to the tunnel centers and relaxed again to determine their structural effects. Table 1 reveals that the calculated cell volume increases by 0.30% and 0.32% in the presence of K^+ and Ba^{2+}, respectively. This increase is caused by enlarging the cell size in the c direction. The cell sizes in the other two directions remain relatively unchanged from the undoped cell. In contrast, the presence of Na^+ shrinks the cell volume by 0.17%, as a result of reducing the cell size in the a direction. As seen in Fig. 1, we found two high-symmetry sites along the (2×2) tunnel: Sites A and B. The lower-energy position (*i.e.*, the more stable) for the

cation is Site A, which neighbors with eight oxygen atoms. The α-MnO_2 cell volume increase in the presence of K^+ and Ba^{2+} causes the slightly longer distances between the cation and its closest Mn and O than those for Na^+ (Table 1).

To analyze the cation – α-MnO_2 interaction, the binding energy E_b of a cation is defined as:

$$E_b = \frac{E_{tot,doped} - E_{tot,undoped} - nE_{dopant}}{n} \quad (1)$$

where $E_{tot,doped}$ and $E_{tot,undoped}$ are the total energy of $Mn_{24}O_{48}$ doped with and without a cation, respectively. E_{dopant} is the energy of an individual K, Na, or Ba atom, and n is the number of cations in the cell.[9,34] E_b between cation and α-MnO_2 is 4.48eV/K^+, 4.18 eV/Na^+, and 8.34eV/Ba^{2+}, indicating a strong interaction. Ba^{2+} donates more valence electrons to α-MnO_2, leading to much higher E_b than that of K^+ and Na^+. Interestingly, the same-charged cations K^+ and Na^+ also have slightly different E_b.

It is worth noting that during synthesis of these compounds, H_2O molecules can be found to coordinate with the cation and hinder CO_2 adsorption uptake [26,34]. However, in a previous experimental study of K-doped OMS-2, it has been shown that upon heating to 150°C, the H_2O can be removed without affecting the K^+ dopant [34]. This is likely due to the difference in binding energy between the H_2O molecule (0.39 eV) and the K^+ dopant (> 4 eV) in α-MnO_2 [34]. Given that the other cations investigated in this study have similar or greater binding energies than K^+, it is reasonable to assume the same ease of H_2O removal from their compounds as well.

Adding a cation to α-MnO_2 also reduces Mn^{4+} to Mn^{3+}.[34,38] Our calculations showed that each donated electron is shared by several Mn, resulting in non-integer charges on the Mn. We calculated the electronic structures of undoped and doped α-MnO_2 and compared them to provide detailed insight into the cation effect on the molecular orbitals of the α-MnO_2. Fig 2(a) – (c) shows the DOS (density of states) of α-MnO_2 doped with K, Na, and Ba, compared with the DOS of K, Na, and Ba individually. The Fermi energy is zero in each case. Undoped α-MnO_2 is a semiconductor with a band gap of 1.33 eV (see the DOS of undoped α-MnO_2 in Fig 2(d)). In the presence of a cation, the conduction band of α-MnO_2 is shifted below the Fermi energy at zero due to the accumulated electrons from the cation, leading to the n-type conduction and the ionic characteristics of the cation – α-MnO_2 bonds. For K and Ba doping, molecular orbital hybridization also occurs on the higher energy level between -13 eV and -12 eV, indicating the covalent characteristics of the cation – α-MnO_2 bonds. This feature explains the binding energy, E_b, difference for K^+ and Na^+ in α-MnO_2. Fig 2(d) combines the DOS curves of doped and undoped α-MnO_2. Cation doping can minimize the band gap of α-MnO_2. Ba doping provides the calculated band gap of 1.14 eV, smaller than 1.29 eV with K doping. Experimentally, the band gap for cryptomelane, *i.e.* α-MnO_2 with K^+, is 1.32 eV [39], agreeing well with our calculations.

<u>CO_2 Sorption</u>

CO_2 adsorption in the OMS-2 tunnel more greatly affects the structure of α-MnO_2 than cation doping does. Table 2 shows that this effect is larger for the K- and Ba-doped systems with cell volume increases of 1.00% and 0.97%, respectively. The Na-doped system is the least affected with a cell volume increase of only 0.63%. However, the CO_2 adsorption enlarges the volume change by three times more than the cation-doped system without CO_2.

Cations are distributed along the OMS-2 (2×2) tunnel. When CO_2 diffuses in the tunnel and encounters a cation, there are three possible scenarios (Fig. 3). For different cations, we estimated an activation energy barrier for each scenario. The lower activation energy barrier represented the more favorable scenario for the cation.

- Scenario I: CO_2 does not continue diffusing, and it remains in a stable position.
- Scenario II: CO_2 continues diffusing, and it can bypass a cation.
- Scenario III: CO_2 continues diffusing, and it can push a cation away.

With a low concentration of CO_2 in the K-doped OMS-2 (averagely $KMn_{24}O_{48}$ with one CO_2 molecule), CO_2 is kinetically trapped in a position away from a K^+ cation with the equilibrium distance of 3.0Å. Due to a high activation energy barrier of ~6eV/CO_2, CO_2 remains in the equilibrium position without further diffusion (Scenario I,

Fig 3(a)). As the concentration of CO_2 increases, the activation energy barrier minimizes to 0.13 eV/CO_2 [26], smaller than a diffusion energy barrier of 0.37 eV for a K^+ cation. These computational results suggest Scenario II (Fig 3(b)), where CO_2 bypasses a K^+ cation to further diffuse along the OMS-2 tunnel when CO_2 has a high concentration (averagely $KMn_{24}O_{48}$ with two or more than two CO_2 molecules). The reduction in activation energy barrier indicates that at elevated CO_2 partial pressures, the transition state becomes more energetically favorable [26].

In the Ba-doped OMS-2, the activation energy barrier for CO_2 diffusion decreases from 6.87eV/CO_2 to 1.02eV/CO_2 due to the CO_2 concentration increase, but the barrier is still higher than that in the K-doped OMS-2. It is not low enough to be overcome. Thus, CO_2 is stuck in the optimum position with a distance of ~3Å (Scenario I). No further diffusion occurs. This mechanism suggests worse CO_2 uptake performance of the Ba-doped OMS-2.

The cell volume of α-MnO_2 increases with the K and Ba doping, but it decreases with the Na doping. In addition, the Na - α-MnO_2 binding energy is the smallest, compared to those for K^+ and Ba^{2+}. These features imply a different CO_2 sorption mechanism occurs in the Na-doped OMS-2. We estimated the adsorption energy of CO_2 in the OMS-2 by modifying Equation (1) in order to study the cation effect on the CO_2 adsorption performance. If the adsorption energy of CO_2 is a positive value, adsorbing CO_2 costs an energy penalty, *i.e.* an increase in the total energy of the system. If the adsorption energy of CO_2 is a negative value, adsorbing CO_2 is energetically favorable, *i.e.* a decrease in the total energy of the system. In comparison between the K- and Na-doped OMS-2, we obtained 0.89eV/CO_2 and -0.61eV/CO_2, respectively. The negative and lower CO_2 adsorption energy suggests that the Na-doped OMS-2 should display higher CO_2 uptake capacity than the K-doped OMS-2. However, a large amount of CO_2 uptake in the OMS-2 reduces the spaces available for additional CO_2, leading to the adsorption energy increase. We found that the high concentration of CO_2 in the Na-doped OMS-2 (*e.g.*, $NaMn_{24}O_{48}$ with two or more than two CO_2 molecules) causes the adsorption energy to increase from -0.61 eV/CO_2 to 0.83eV/CO_2. Therefore, increasing temperature or pressure is needed to facilitate the CO_2 adsorption process.

After adsorption, CO_2 diffuses in the OMS-2 tunnel until it encounters a Na^+ cation with an equilibrium distance of 3.81 Å (Scenario I), longer than with a K^+ cation. The cation behaves as a "gate keeper" to block further CO_2 diffusion. Considering Scenario II, as in the K-doping case, CO_2 bypasses the Na^+ cation. It has to form an unstable transition configuration, where CO_2 sits by the side of the cation, and the cation slightly shifts to the OMS-2 porous surface to give more space to CO_2 (Fig. 3(b)). With a low concentration of CO_2, the transition configuration experiences an activation energy barrier of 3.04 eV/CO_2 for the Na-doped OMS-2, about three times smaller than that for the K-doped OMS-2. As the concentration of CO_2 increases, the activation energy barrier reduces to 0.87 eV/CO_2, but it is still too high to overcome. Therefore, Scenario II is not kinetically favorable.

In Scenario III, CO_2 pushes the cation along the OMS-2 tunnel axis (Fig. 3(C)). The energy required to displace the cation, which is calculated as the difference in total energy between the system where the cation is in its equilibrium position and that of the cation in the adjacent position, is referred to as the 'diffusion energy.' This mechanism requires a sufficiently low energy barrier for the cation. We estimated the diffusion energy barrier of 0.16 eV for the Na^+ cation in the OMS-2 tunnel. Such a value can be easily overcome, and is much smaller than both the activation energy barrier for CO_2 to bypass the Na^+ cation as well as the diffusion energy barrier for the K^+ cation. Research on porous materials exhibited that the cation is movable in the porous tunnels [9,26,40,41]. Our calculations indicate that Scenario III is more energetically favorable, where CO_2 pushes the Na^+ cation to further diffuse along the OMS-2 tunnel.

Table 3 summarizes different CO_2 sorption mechanisms in the OMS-2 with K, Na, and Ba doping. Scenario I occurs in all three cases. After adsorption, CO_2 is thermally activated to diffuse in the OMS-2 tunnel until it encounters a cation. For a K^+ cation, CO_2 bypasses it to further diffuse along the OMS-2 tunnel (Scenario II). For a Na^+ cation, CO_2 continues diffusing by pushing the cation (Scenario III). These scenarios are illustrated in Figure 3. For a Ba^{2+} cation, CO_2 remains in an optimum position with no further diffusion. These mechanisms suggest a sorption hysteresis. The phenomenon of sorption hysteresis commonly occurs in gas molecule adsorption and desorption isotherms. This indicates that the path to adsorption of gas molecules by a porous host differs from that of desorption.

Even though it has the worst CO_2 uptake capacity, the Ba-doped OMS-2 is expected to have the smallest hysteresis. Upon desorption (*e.g.*, a pressure decrease) CO_2 can easily exit the OMS-2 tunnel. In contrast, CO_2 can diffuse farther in the OMS-2 tunnel by passing through a K^+ cation and pushing a Na^+ cation. These mechanisms require a

longer time to vacuum CO_2 in the OMS-2 tunnel, yielding the phenomenon of sorption hysteresis. The Na-doped OMS-2 should have a slightly smaller hysteresis than the K-doped OMS-2. In Scenario II, upon desorption CO_2 has to pass through the K^+ cation in reverse. This action costs an energy penalty and requires more time than the Na^+ cation case, where CO_2 can directly exit the tunnel with no need to pass any Na^+ cation. The computational prediction has been validated by our experiment, which will be published in another experimental paper soon. Our results suggest that the charge, size and mobility of cation accommodated in a porous material control the CO_2 uptake capacity and sorption hysteresis.

IV. Conclusions

We have performed first-principles quantum mechanical simulations, based on density functional theory incorporated with van der Waals interaction (DFT+vdW), to study cation effects on the OMS-2 structure and CO_2 sorption. K^+, Na^+, and Ba^{2+} cations have to be accommodated in the OMS-2 tunnel for structural stability. The charge and type of the cation affect the OMS-2 structure where the K^+ and Ba^{2+} cations lead to a cell volume increase while the Na^+ cation decreases the cell volume. Conversely, the like-charge K^+ and Na^+ cations have the smaller binding energies with the porous surface of the OMS-2 than the higher-charged Ba^{2+} cation. Besides the charge and type, cation mobility is also found to control the CO_2 uptake capacity and sorption mechanism of OMS-2. The diffusion of adsorbed CO_2 is hindered by the cations, which act as 'gatekeepers' blocking the CO_2 diffusion. It traps CO_2 within the OMS-2 leading to a sorption hysteresis. After adsorption, CO_2 diffuses until it encounters a cation. Three possible mechanisms occur, depending on an activation energy barrier for further CO_2 diffusion and cation mobility. Scenario I involves CO_2 becoming kinetically trapped in an equilibrium position with no further diffusion. Scenario II is that CO_2 bypasses the cation to further diffuse along the OMS-2 tunnel. Scenario III is that CO_2 continues diffusing by pushing the cation away. In all three cation cases, Scenario I occurs. In the K- and Na-doped OMS-2, CO_2 can diffuse further through Scenarios II and III, respectively. These mechanisms also suggest that the Ba-doped OMS-2 should have the smallest sorption hysteresis, followed by the Na-doped OMS-2, and finally the K-doped OMS-2. Our studies provide detailed insights into the interactions between cations and OMS-2 and the CO_2 sorption performance of OMS-2. The results reveal that CO_2 uptake capacity and sorption hysteresis can be optimized by changing the cations accommodated in the porous materials, which is important to develop effective and efficient CO_2 capture and storage materials.

Acknowledgments

This work was partially funded by the NIST-ARRA fellowship. The authors would like to thank Eric Cockayne, Laura Espinal, and Winnie Wong-Ng at NIST for computational and experimental consultations. The calculations in this paper were performed on the high-performance computing systems at Idaho National Lab and Boise State University.

Table 1. Effect of cation on the structural features of α-MnO2, including lattice parameters (Å) and cell volume (Å^3).

	Cell Parameters, *a*, *b*, *c* (Å)			Volume (Å^3)	Bond length (Å)	
Pure $Mn_{24}O_{48}$	9.702	8.568	9.685	805.04		
With Cation					Cation-Mn	Cation-O
K^+	9.702	8.554	9.731	807.48	3.57	2.85
Na^+	9.678	8.555	9.706	803.63	3.55	2.82
Ba^{2+}	9.713	8.542	9.735	807.64	3.59	2.83

Table 2. Effect of CO_2 sorption on the structural features of α-MnO_2, including lattice parameters (Å) and cell volume (Å^3)

	Cell Parameters, *a*, *b*, *c* (Å)			Volume (Å^3)	Volume Change
Pure $Mn_{24}O_{48}$	9.702	8.568	9.685	805.04	--
With Cation and CO_2 Adsorption					
$KMn_{24}O_{48}$+CO_2	9.797	8.545	9.712	813.06	1.00%
$NaMn_{24}O_{48}$+CO_2	9.735	8.557	9.725	810.13	0.63%
$BaMn_{24}O_{48}$+CO_2	9.747	8.536	9.769	812.83	0.97%

Table 3. Summary of three CO_2 diffusion mechanisms for corresponding cations

	Scenario I	Scenario II	Scenario III
K-doped OMS-2	✓	✓	
Na-doped OMS-2	✓		✓
Ba-doped OMS-2	✓		

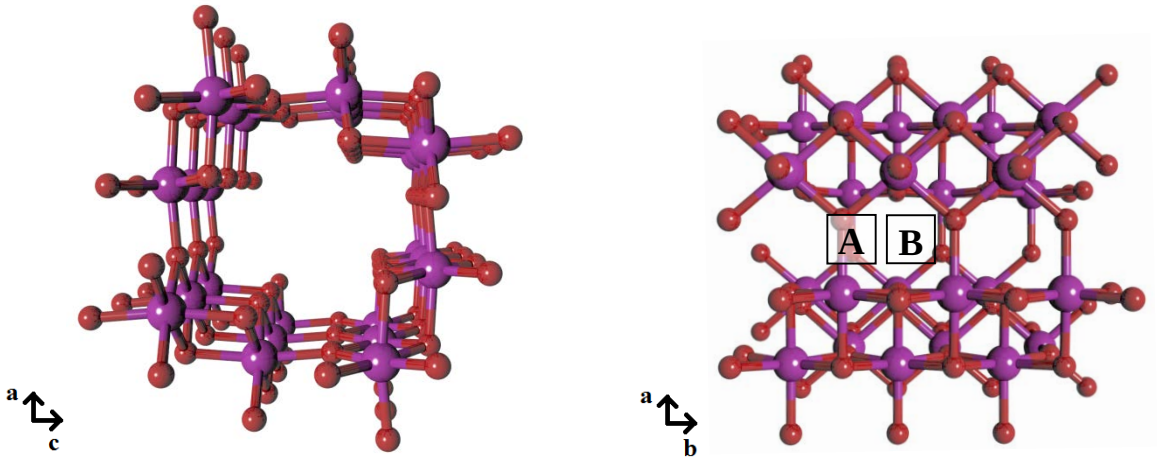

Fig. 1 Different views of a crystal structure of α-MnO_2, where Mn is purple, and O is red. The (2×2) tunnel is along the *b* axis. Sites A and B are two high-symmetry positions.

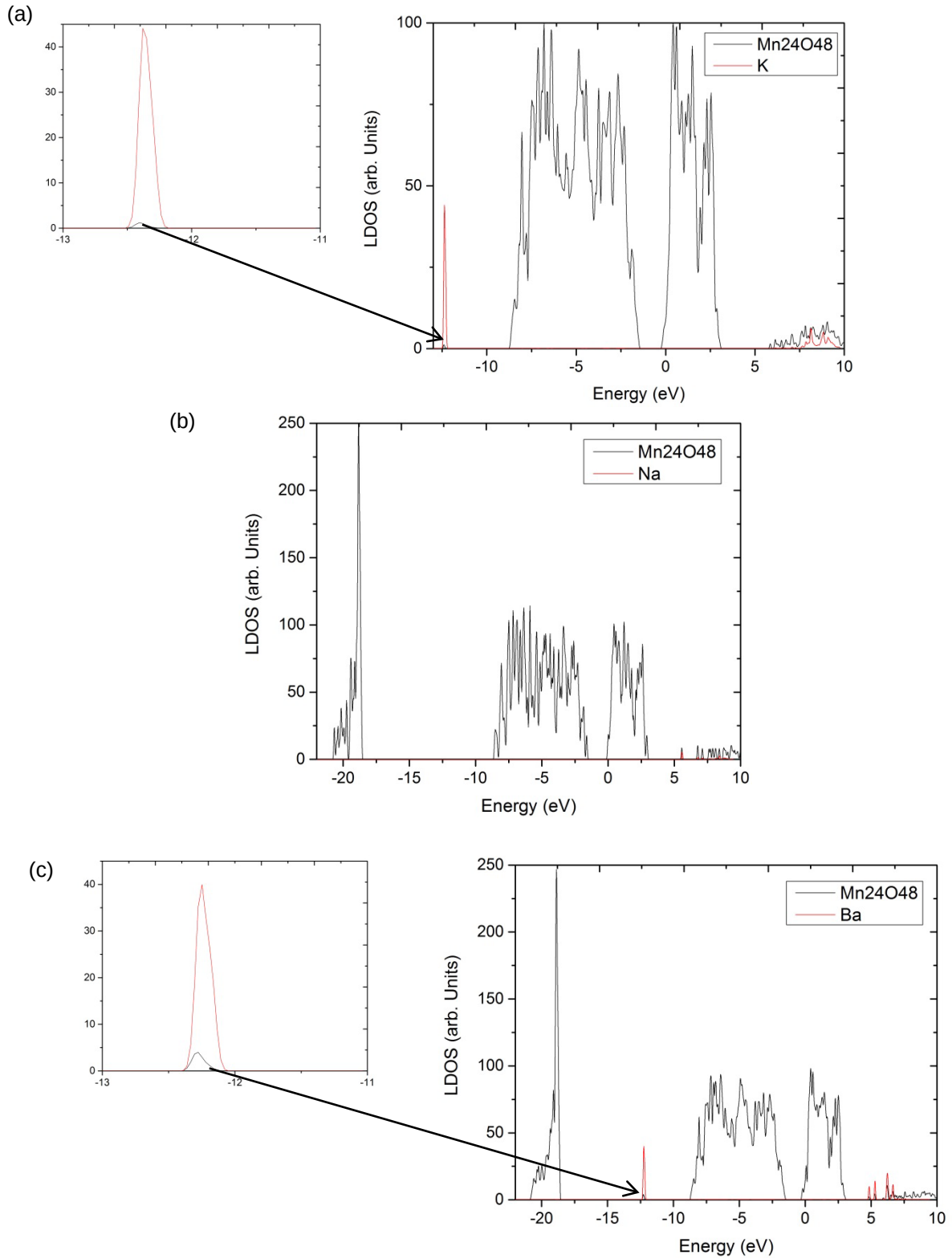

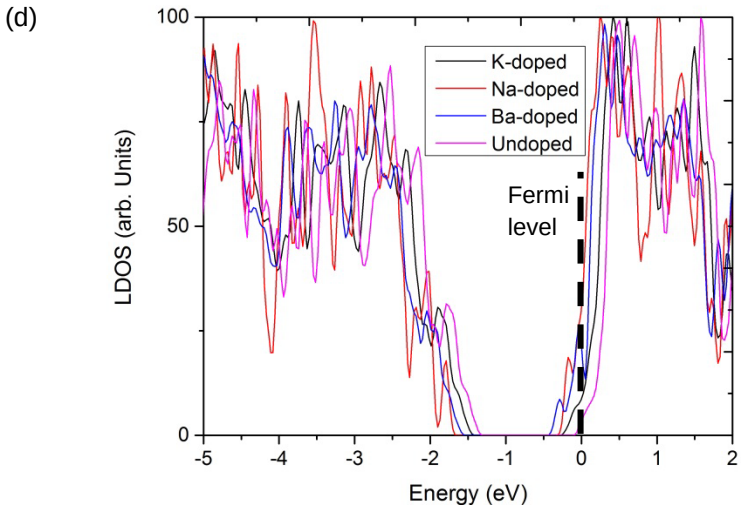

Fig. 2 Density of states (DOS) for doped and undoped α-MnO_2. (a)-(c) DOS projected on α-MnO_2, K, Na, and Ba individually; and (d) DOS comparison before and after doping in α-MnO_2.

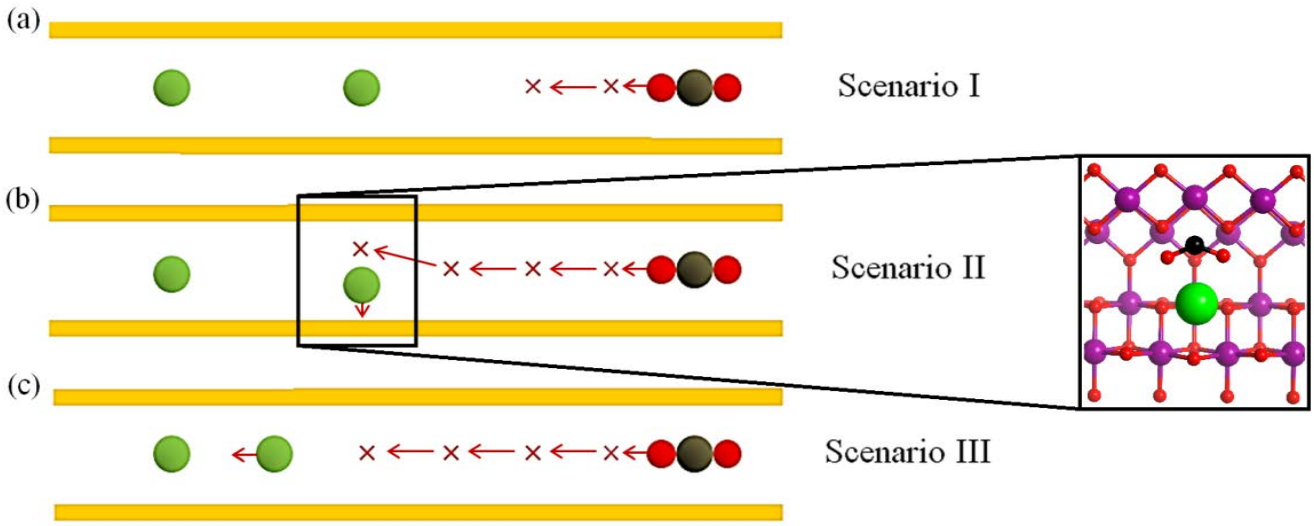

Fig. 3 Three possible diffusion mechanisms for CO_2 in an OMS-2 (2×2) tunnel: red, O; black, C; green, cation (K^+, Na^+, or Ba^{2+}); red cross, corresponding CO_2 position; red arrow, diffusion direction. For clarity, yellow walls highlight the location of the MnO_2 (tunnel walls). (a) CO_2 remains an optimum distance from the cation (Scenario I); (b) CO_2 bypasses a cation while the cation shifts towards the porous surface (Scenario II), the insert depicts the transition state in the OMS-2 tunnel where the CO_2 molecule sits alongside the cation and the O-C-O angle is distorted to 134.5° (foreground atoms removed for clarity); and (c) CO_2 pushes a cation to diffuse (Scenario III). There is an activation energy barrier associated with the formation of the transition state in Scenario II and a diffusion energy barrier for the CO_2 to push the cation in Scenario III.

References

[1] S. Chu, Science 325 (2009) 1599.
[2] Y. Cui, H. Kita, K. Okamoto, Chem Commun 17 (2003) 2154.
[3] Q.L. Liu, A. Mace, Z. Bacsik, J.L. Sun, A. Laaksonen, N. Hedin, Chem Commun 46 (2010) 4502.
[4] J.R. Li, R.J. Kuppler, H.C. Zhou, Chem Soc Rev 38 (2009) 1477.
[5] L.C. Lin, K. Lee, L. Gagliardi, J.B. Neaton, B. Smit, J Chem Theory Comput 10 (2014) 1477.
[6] J.R. Li, Y.G. Ma, M.C. McCarthy, J. Sculley, J.M. Yu, H.K. Jeong, P.B. Balbuena, H.C. Zhou, Coordin Chem Rev 255 (2011) 1791.
[7] D. Britt, H. Furukawa, B. Wang, T.G. Glover, O.M. Yaghi, P Natl Acad Sci USA 106 (2009) 20637.
[8] L. C. Lin, A. H. Burger, R. L. Martin, J. Kim, J. A. Swisher, K. Jariwala, C. H. Rycroft, A. S. Bhown, M. W. Deem, M. Haranczyk, B. Smit, Nat Mater 11 (2012) 633.
[9] L. Li, E. Cockayne, I. Williamson, L. Espinal, W. Wong-Ng, Chem Phys Lett 580 (2013) 120.
[10] Z.B. Bao, L.A. Yu, Q.L. Ren, X.Y. Lu, S.G. Deng, J Colloid Interf Sci 353 (2011) 549.
[11] Z.R. Herm, R. Krishna, J.R. Long, Micropor Mesopor Mat 157 (2012) 94.
[12] J. Seo, D. Whang, H. Lee, S. Jun, J. Oh, Y. Jeon, K. Kim, Nature 404 (2000) 982.
[13] A.J. Brown, N.A. Brunelli, K. Eum, F. Rashidi, J.R. Johnson, W.J. Koros, C.W. Jones, S. Nair, Science 345 (2014) 72.
[14] J. Gascon, F. Kapteijn, B. Zornoza, V. Sebastián, C. Casado, J. Coronas, Chem. Mater. 24 (2012) 2829.
[15] H. Li, M. Eddaoudi, M. O'Keeffe, O.M. Yaghi, Nature 402 (1999) 276.
[16] K.G. Ray, D.L. Olmsted, J.M.R. Burton, Y. Houndonougbo, B.B. Laird, M. Asta, Chem Mater 26 (2014) 3976.
[17] P. Canepa, C.A. Arter, E.M. Conwill, D.H. Johnson, B.A. Shoemaker, K.Z. Soliman, T. Thonhauser, J Mater Chem A 1 (2013) 13597.
[18] P. Canepa, N. Nijem, Y.J. Chabal, T. Thonhauser, Phys Rev Lett 110 (2013) 026102.
[19] C. Lastoskie, K.E. Gubbins, N. Quirke, J Phys Chem-Us 97 (1993) 4786.
[20] D.L. Bish, J.E. Post, Am Mineral 74 (1989) 177.
[21] R.N. Deguzman, Y.F. Shen, E.J. Neth, S.L. Suib, C.L. O'young, S. Levine, J.M. Newsam, Chem Mater 6 (1994) 815.
[22] S.L. Suib, Accounts Chem Res 41 (2008) 479.
[23] W. Morris, N. He, K.G. Ray, P. Klonowski, H. Furukawa, I.N. Daniels, Y.A. Houndonougbo, M. Asta, O.M. Yaghi, B.B. Laird, Journal of Physical Chemistry C 116 (2012) 24084.
[24] X. Chen, Y.F. Shen, S.L. Suib, C.L. O'Young, J Catal 197 (2001) 292.
[25] S.L. Suib, J Mater Chem 18 (2008) 1623.
[26] L. Espinal, W. Wong-Ng, J.A. Kaduk, A.J. Allen, C.R. Snyder, C. Chiu, D.W. Siderius, L. Li, E. Cockayne, A.E. Espinal, S.L. Suib, J Am Chem Soc 134 (2012) 7944.
[27] A. Bystrom, A.M. Bystrom, Acta Crystallogr 3 (1950) 146.
[28] G. Kresse, J. Furthmuller, Phys Rev B 54 (1996) 11169.
[29] J.P. Perdew, A. Ruzsinszky, G.I. Csonka, O.A. Vydrov, G.E. Scuseria, L.A. Constantin, X.L. Zhou, K. Burke, Phys Rev Lett 100 (2008) 136406.
[30] P.E. Blochl, Phys Rev B 50 (1994) 17953.
[31] G. Kresse, D. Joubert, Phys Rev B 59 (1999) 1758.
[32] A.I. Liechtenstein, V.I. Anisimov, J. Zaanen, Phys Rev B 52 (1995) R5467.
[33] Y. Paik, J.P. Osegovic, F. Wang, W. Bowden, C.P. Grey, Journal of the American Chemical Society 123 (2001) 9367.
[34] E. Cockayne, L. Li, Chem Phys Lett 544 (2012) 53.
[35] S. Grimme, Journal of computational chemistry 27 (2006) 1787.
[36] H. Wu, J.M. Simmons, G. Srinivas, W. Zhou, T. Yildirim, J Phys Chem Lett 1 (2010) 1946.
[37] M.K. Rana, H.S. Koh, J. Hwang, D.J. Siegel, Journal of Physical Chemistry C 116 (2012) 16957.
[38] A. Iyer, H. Galindo, S. Sithambaram, C. King'ondu, C.-H. Chen, S.L. Suib, Applied Catalysis A: General 375 (2010) 295.
[39] T. Gao, M. Glerup, F. Krumeich, R. Nesper, H. Fjellvag, P. Norby, J. Phys. Chem. C 112 (2008) 13134.
[40] J. Lan, D. Cao, W. Wang, B. Smit, ACS Nano 4 (2010) 4225.
[41] H. Pfeiffer, C. Vázquez, V.H. Lara, P. Bosch, Chem. Mater. 19 (2007) 922.